Plant-based synthesis of NiO nanoparticles using salvia macrosiphon Boiss extract and examination of their water treatment

Zahra Sabouri, Narges Fereydouni, Alireza Akbari, Hasan Ali Hosseini, Alireza Hashemzadeh, Mohammad Sadegh Amiri, Reza Kazemi Oskuee, Majid Darroudi* ⓘ

Abstract The goal of this study was to synthesize nickel oxide nanoparticles (NiO-NPs) by the sol–gel method, which involved the use of salvia macrosiphon Boiss plant extract, $Ni(NO_3)_2 \cdot 6H_2O$ as a capping agent, and a nickel precursor, respectively. The synthesized NiO-NPs were characterized by Fourier transform infrared spectroscopy (FTIR), ultraviolet–visible (UV–Vis) spectrophotometer, X-ray diffraction (XRD), field electron scanning electron microscopy (FESEM)/energy-dispersive X-ray spectroscopy (EDX), thermo-gravimetric analysis/differential thermal analysis (TGA/DTA) and vibrating sample magnetometer (VSM) analyzes. Also, according to the results of UV–Vis, the gap band of nanoparticles was calculated to be in the range of about 2.9–3.9 eV. The photocatalytic activity of nanoparticles on methylene blue (MB) degradation was investigated and according to the results, about 80% MB was apparently degraded in the presence of NiO-NPs under UV-A light (11 W) after 5 h in pH $\sim$ 11. We have evaluated the cytotoxicity of NiO-NPs on the multiple tumor cells by materials method, and all the utilized concentrations were observed to cause non-toxic effects; therefore, it can be suggested that these samples have the potential of being employed in different fields of medicine.

Keywords Nickel oxide nanoparticles; Sol–gel; Photocatalytic degradation; Salvia macrosiphon Boiss plant extract; Cytotoxicity

Z. Sabouri, A. Akbari, H. A. Hosseini
Department of Chemistry, University of Payame Noor, Tehran 19395-4697, Iran

N. Fereydouni
Neurogenic Inflammation Research Center, University of Medical Sciences, Mashhad 9177948564, Iran

A. Hashemzadeh
NanoBioEletrochemistry Research Center, University of Bam Medical Sciences, Bam 7661713669, Iran

M. S. Amiri
Department of Biology, University of Payame Noor, Tehran 19395-4697, Iran

R. Kazemi Oskuee
Targeted Drug Delivery Research Center, Institute of Pharmaceutical Technology, University of Medical Sciences, Mashhad 9177948564, Iran

M. Darroudi*
Nuclear Medicine Research Center, University of Medical Sciences, Mashhad 9177948564, Iran
e-mail: darroudim@mums.ac.ir; majiddarroudi@gmail.com

M. Darroudi
Department of Modern Sciences and Technologies, School of Medicine, University of Medical Sciences, Mashhad 9177948564, Iran

1 Introduction

In recent years, nanostructured materials have attracted a lot of attention due to their interesting and unique properties. Among various nanoscale materials, metal oxides have been focused on by many researchers since they contain fascinating features, such as being optical, magnetic, electrical and catalytic, along with general qualities such as thermal stability and chemical properties when compared to their bulk state. In the meantime, NiO is an important oxide due to its chemical and magnetic properties [1]. This material is known to be antiferromagnetic and by decreasing its particle size, it will be able to exhibit

superparamagnetic and weak ferromagnetic properties [2]. Also, due to their anti-inflammatory features, nickel oxide nanoparticles (NiO-NPs) have been utilized in the field of biomedicine. NiO is a p-type semiconductor with an extensive band gap that had been observed to be in the range of 3.6–4.0 eV [3, 4]. NiO-NPs contain many applications in the fields of conductive colors, catalysis [4, 5], anticancer [6], optoelectronics [7], magnetic recording devices [8], ferromagnetic fluids [9], modified electrodes [10], fuel cells [11, 12], ultraviolet absorber [13], magnetic resonance imaging with a high contrast, medicine and drug delivery [14], gas sensors [15], battery cathodes [16] and electroceramic films [17]. A number of preparation approaches were suggested for the manufacture of NiO-NPs, which involves solid-state method [18, 19], hydrothermal [20, 21], coprecipitation [22], sonochemical [23], microwave-assisted heating [24], laser chemical method [25] and sol–gel [26, 27]. In the current research, the sol–gel method was employed due to its advantages such as being capable of producing super pure powders, lack of requiring complex laboratory equipment, being simple and inexpensive [28] and facilitating the industrial production of nanoparticles with a great specific surface region at low temperature [29, 30]. In recent researches, photocatalytic degradation has been offered as an economical way for eliminating the dyes and pollutants of wastewater through the application of metal oxide semiconductors including CuO, ZnO, TiO$_2$ and NiO [31–33]. The individual qualities of NiO, such as being economical and non-toxicant, as well as containing photostability and easy availability [34], have labeled this substance as an effective photocatalyst for the degeneration of several organic pollutants [18, 35]. The increasing environmental contamination has absorbed the attention of global investigators on the topic of developing effective photocatalysts, which are centered on semiconductors for the treatment of contaminated water resources by various organic pollutants that are released from many different industries [36, 37]. The photocatalysis of semiconductors can be caused by the electron–hole pairs later band-gap excitation. Although a photocatalyst can be explained with light and energy that is equivalent or bigger than the band-gap energy, the valence band electrons become excited by the conduction band, which results in a positive hole in the valence band as it is exhibited in the following [38].

$$\text{Photocatalyst(e.g., NiO)} \xrightarrow{hv} e_{CB}^- + h_{VB}^+ \qquad (1)$$
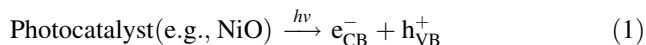
Hence, in the current research, NiO-NPs have been prepared by a novel, simple, safe, available, eco-friendly [39] and green procedure that involves the usage of salvia plant extract as a capping and stabilizing agent to prevent the stimulus of aggregations among nanoparticles [40, 41].

The tissues of plant seeds can function as bio-templates for the purpose of detecting the dimension of nanoparticles and hinder their agglomeration [42]. Although a lot of researches have been carried out on the synthesizing method and photocatalytic effects of NiO-NPs, yet there are few reports on the usage of salvia plant extract throughout the synthesizing process, in which it functions as the capping agent in scientific resources. Therefore, one of the advantages of our work in comparison with others is the utilization of least possible amount of catalysts (3 mg) under a low-intensity UV-A light source (11 W). Despite these conditions, the degradation efficiency has been observed to reach about 80%. The goal of this research was to develop an eco-friendly and economical method for performing the biosynthesis of NiO-NPs by the usage of salvia macrosiphon Boiss plant extract, as well as examining the photocatalytic effect of NiO-NPs on eliminating the methylene blue (MB) dye of an aqueous environment and achieving a higher degradation efficiency (80%) of NiO-NPs for the degradation of MB. In the following, the anticancer properties of nanoparticles on Neuro2A cells were investigated by the usage of the materials method and in the end, the nanoparticles were characterized through the modern spectroscopy techniques.

2 Experimental

2.1 Chemicals

Compounds with great clarity were purchased from Sigma-Aldrich and used without any further purification. Double distilled water was utilized throughout all the involved experiments as a solvent. The raw materials included Ni (NO$_3$)$_2$·6H$_2$O (98%, Sigma-Aldrich), salvia plant extract that was collected from the natural habitats and methylene blue (MB; 98%, Sigma-Aldrich) dye.

2.2 Apparatus

An ultraviolet–visible (UV–Vis) spectrophotometer (Shimadzu, Japan) with quartz cells was used to measure the adsorption, a magnetic stirrer and a heater to stir the appointed solutions, a UV-A lamp 11 W to perform the photocatalyst test and a pH meter to control the pH.

2.3 Characterization techniques of NiO-NPs

Characterization of nanoparticles stands as the most important factor in comprehending and controlling the synthesis and application of nanoparticles. This vital factor can be achieved by utilizing a variety of procedures including X-ray diffraction (XRD, D8-Advance Bruker),

Fourier transform infrared spectroscopy (FTIR, Shimadzu), UV–Vis, field electron scanning electron microscopy (FESEM)/energy-dispersive X-ray spectroscopy (EDX, Tescan Brno-Mira3 Lmu), vibrating sample magnetometer (VSM, MDKB) and thermo-gravimetric analysis/differential thermal analysis (TGA/DTA, BAHR STA 503).

2.4 Plant collection and extraction

The salvia plant used in this research was collected from the natural habitats around the cities of Tabas and Sabzevar, Iran. Then, their different parts, such as air sections (branches and leaves), fruit and roots, were washed by the usage of deionized water in satisfying conditions and dried in dark. The powdering process was performed by the means of an electric mill to prepare the designated extract. Thereafter, 20.0 g plant powder was dissolved in 100 ml water and stirred at the temperature of 60 °C for 3 h; as the following step, the resultant was filtered and centrifuged for the purpose of removing the remaining impurities. The final product was stored in the refrigerator at 4 °C to be utilized in the upcoming steps.

2.5 Biosynthesis of NiO-NPs

To perform the synthesizing process of NiO-NPs in the present work, 7.5 g $Ni(NO_3)_2 \cdot 6H_2O$ was dissolved in 50 ml H_2O and stirred for 30 min at ambient temperature. Then, 30 ml salvia extract was added dropwise to the $Ni(NO_3)_2 \cdot 6H_2O$ solution to achieve a clear brown solution. Afterward, the obtained sol was stirred for the duration of 6 h with a magnetic stirrer at a constant temperature of 80 °C. Finally, a green and slurry gel was observed to remain at the dish, which was dried at a temperature of 180 °C for 2 h. The dried gel was divided into four parts and put into calcination for 2 h at the temperatures of 300, 400, 500 and 600 °C to obtain a black powder. The achieved final product was

Fig. 1 Schematic of biosynthesis of NiO-NPs

confirmed to be NiO-NPs as we demonstrated a schematic of the performed biosynthesis test in Fig. 1. The photocatalytic performance of NiO-NPs was estimated by observing the induced revision of variation in regard to the absorption of methylene blue (MB) solution at ~ 663 nm in the pH of about 9, which was carried out through the photocatalytic decomposition route under UV-A lamp 11 W radiation. In the course of a common experiment, 3×10^{-3} g NiO-NPs was dispersed into 50 ml MB solution (10^{-5} mol·L^{-1}). Beforehand, the container was positioned under a UV light while being stirred in dark for the duration of about 90 min to obtain an adsorption–desorption equilibrium. Afterward, the solution was placed under the UV light for a period of 30 min; the absorbance of MB was measured through the usage of UV–Vis spectrophotometer.

2.6 Evaluation of cytotoxicity effect of NiO-NPs by MTT assay

NiO-NPs, which were synthesized by the means of salvia plant extract, were evaluated through the MTT method for their in vitro cytotoxic activities on the Neuro2A cells. In summary, Neuro2A cells were seeded (1×10^4 cells per well) in 96-well plates and kept protected for a period of 24 h. Subsequent to this duration, the Neuro2A cells were assumed to be affected by various concentrations of nanomaterial in the corporation of 10% fetal bovine serum (FBS). The NiO-NPs were observed to be practical at 500 °C in a 5 µg·ml^{-1} store solution of dimethyl sulfoxide (DMSO) and H_2O. Following the 24-h incubation, 20 µl MTT (3-(4,5-dimethylthiazol-2-yl)-2,5-diphenyltetrazolium bromide, 5 mg·ml^{-1}) was appended to every well in the phosphate-buffered saline (PBS) buffer, while the cells were incubated for 4 h at a temperature of 37 °C. This middle included no reacted dye and was discarded, while 100 µl DMSO was inserted to dissolve the formed crystal that was caused by the surviving cells. The optical absorption was evaluated at 545 nm by the utilization of a microplate reader, while the cytotoxicity was expressed as a percent compared to the natural control cells. As suggested by the observed effects, the metabolic activity faced a reduction in a concentration-dependent manner in regard to the amounts above 15.6 µg·ml^{-1}, indicating that the metabolic activity started to decrease at about 7.8 µg·ml^{-1}, while the maximum point was detected to be at 500 µg·ml^{-1}.

3 Results and discussion

3.1 Photocatalytic evaluation of NiO-NPs

The NiO-NPs calcinated at 500 °C were estimated through their application in the degrading MB under UV light
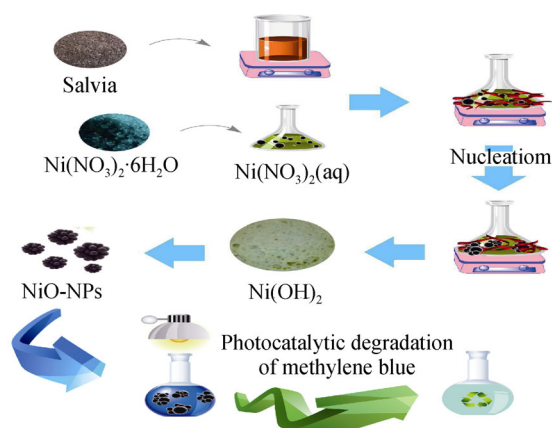
radiation. Apparently, the absorption peak of MB on 663 nm entirely vanished after around 300 min [43]. The percent of degeneration MB dye was estimated by the utilization of Eq. (2).

$$\text{Dyedegradation} = \frac{C_0 - C_t}{C_0} \times 100\% \quad (2)$$

where C_0 and C_t stand for the first concentration of MB and the concentration at any time (t), respectively. The photocatalytic mechanism of NiO-NPs under UV-A light is illustrated in Fig. 2. Subsequent to UV-A light radiation, the existing electrons in the valence band (VB) was excited by the conduction band (CB) of oxide, as well as the associated formation of holes in the VB which resulted in the development of an electron–hole pair. Thereafter, next to the migration of the generated charge at catalyst level, the separation of charges caused the observed redox reactions [44]. Highly reactive hydroxyl radicals can also be fabricated through the disintegration of H_2O [45, 46]; in other words, this particular process requires the reaction of e^- with O_2 in order to gain the $\cdot O_2^-$ and $\cdot HO_2$ on protonation, eventually resulting in further effective $°OH$ radicals. Many different mechanisms suggested in regard to the photocatalytic activities of NiO-NPs [47, 48].

$$UV + NiO \rightarrow NiO^* + h^+ + e^- \quad (3)$$

$$h^+ + MB \rightarrow \cdot MB^+ \quad (4)$$

$$e^- + O_2 \rightarrow \cdot O_2^- \quad (5)$$

$$\cdot O_2^- + H_2O \rightarrow \cdot HO_2 + \cdot OH^- \quad (6)$$

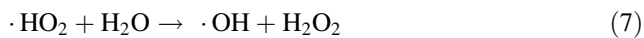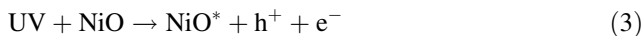$$\cdot HO_2 + H_2O \rightarrow \cdot OH + H_2O_2 \quad (7)$$

Figure 3 illustrates the degeneration rate of MB through the usage of NiO-NPs calcinated at 500 °C, which was detected to be about 80%. The results indicated that the MB degradation was greater compared to the results in the other works [45, 49, 50].
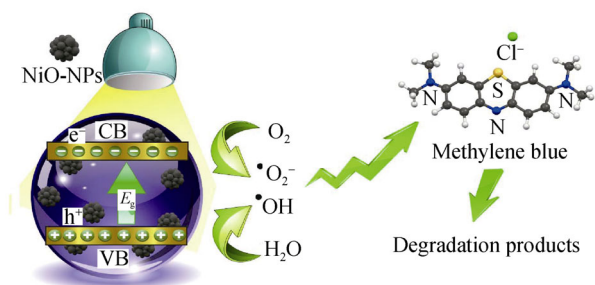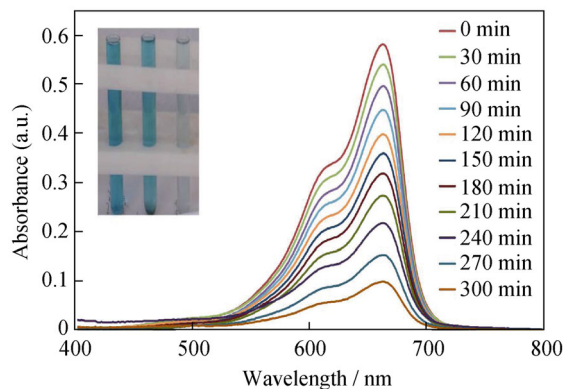

Fig. 3 Degradation of MB by NiO-NPs under UV-A irradiation

3.2 Influences of pH on the photocatalytic degradation of MB in UV/NiO system

pH stands for one of the most important parameters affecting the photocatalytic degradation and throughout this examination, the optimization of pH factor was studied. For this purpose, the pH values of 4, 7 and 9, along with the initial concentration of MB (3.0 mg·L^{-1}) and the photocatalyst concentration (10 mg·L^{-1}), were used while the suspension was exposed to UV-A light (11 W) at the time intervals of 0, 60, 120, 180, 240 and 300 min. The adsorption rate was read through the employment of a spectrophotometer and in the following, the dye degradation efficiency was determined by the application of Eq. (2). The results of MB degradation at different pH values are demonstrated in Fig. 4. As displayed, the amount of photocatalyst degradation increased in the pH of 9, while the MB degradation in pH = 9 was detected to be about 89%. The lowest photocatalytic activity was observed in the acidic environment (pH = 4), which was about 39% [51]. In accordance with the obtained results, the optimum pH for the photodegradation of MB is pH = 9.
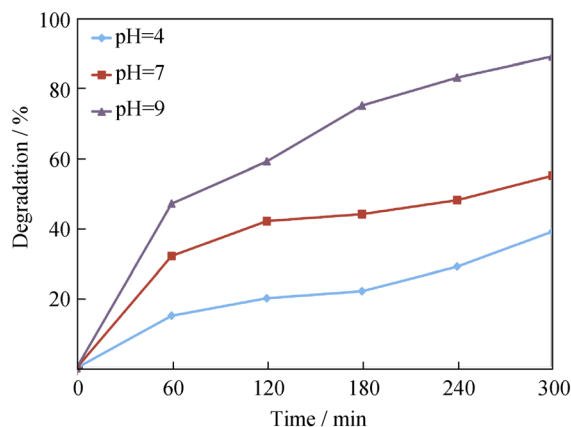

Fig. 2 Schematic representation for degradation of MB on UV light irradiation

Fig. 4 Effect of pH on MB removal with UV/NiO system

3.3 MB photocatalysis destruction kinetics

It can conclude that the disintegration rate of pigment apparently follows a pseudo-first-order kinetic model. Photodegradation of dye has fixed a pseudo-first-order kinetic model which is exhibited in Eq. (8).

$$\ln\left(\frac{C_t}{C_0}\right) = K_{obs}t \tag{8}$$

where C_0 is the concentration ago light, C_t is the concentration at time t and K_{obs} is the obvious rate constant.

Figure 5 demonstrates the graph of $\ln(C_t/C_0)$ versus time of radiation, whereas in regard to MB, the straight line suggests that the process of photon degeneration involves a pseudo-first-order kinetics since the rate constant was detected to be equaled to $k = 0.0047$ min^{-1} [47, 52, 53]. In higher concentrations, the available catalytic sites on the catalyst surface become employed by the adsorbed reactants. The reaction rate was observed to not be dependent on concentration, resulting in zero-order kinetics where K_0 represented the constant of the zero-order rate. In the case of dilute solutions, the reaction rate was concentration dependent, leading to the inducement of first-order kinetics, where K_1 represented the rate constant of the first order at low concentrations; also, considering why the catalytic positions are not limiting factors, the rate of degradation was detected to be proportional to the concentration of pollutants [54, 55].

3.4 TGA/DTA analysis of NiO-NPs

TGA/DTA analysis of nickel hydroxide gel was approved by the application of sol–gel method in nitrogen atmosphere via a heating speed of 10 °C·min^{-1}, and this measurement began at ambient temperature and then heightened up to 1000 °C; the mentioned data are presented in Fig. 6. The four stages of weight loss can be
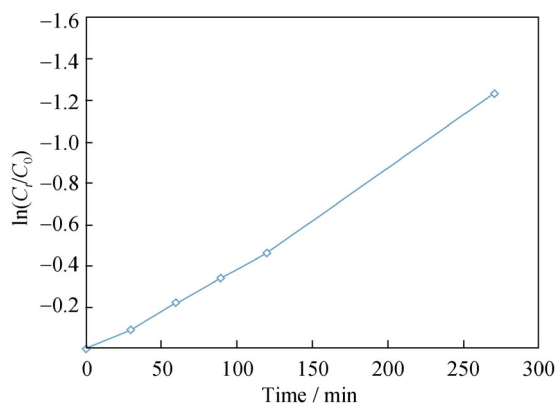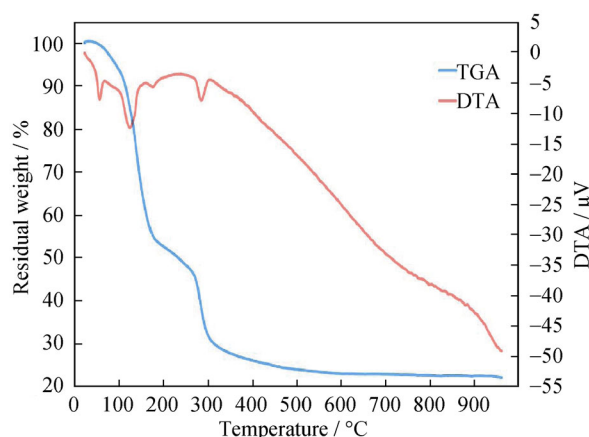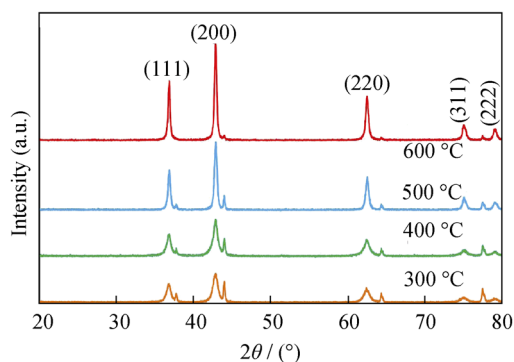
Fig. 6 TGA/DTA curves of initial gel to achieve NiO-NPs

detected in TGA graph, which is apparently accompanied by three endothermic peaks in DTA graph. The first weight loss, detected between 109 °C and 179 °C, was associated with the vaporization of water molecules and the slight removal of hydroxyl group volume that was induced during the transformation phase; this particular weight loss was about 46% [23]. The second weight loss, observed in the range of 179–268 °C, was probably associated with the decomposition of chemically bounded groups, which had been reported to be close to about 8%. The third weight reduction that was noticed to exist between 268 and 310 °C was clearly associated with the breakdown of the carbon-based compound and the creation of pyrochlore phases. The mentioned reduction was reported to be about 16%. The last weight loss step, from 310 to 541 °C, was assigned to the breakdown of pyrochlore phases in addition to the generated NiO pure phases, which was observed to be about 8%. A slow weight loss was also detected in TGA curve, occurring between 310 and 750 °C, which is indicative of a slight removal of hydroxyl group volume during the induced changes of NiO phase. Moreover, a small endothermic peak was perceived in the DTA curve at around 59 °C, which was supposedly caused by the vaporization of the remaining water in the sample [56]. The other two endothermic peaks spotted at 126 and 286 °C may be related to the eliminated water of crystallization and the thermal oxidative decomposition of Ni(OH)$_2$, respectively [56].

3.5 XRD analysis of NiO-NPs

As observed, Fig. 7 illustrates XRD patterns of NiO-NPs. XRD patterns were utilized to evaluate the crystallinity of biosynthesized NiO-NPs prepared through the usage of salvia macrosiphon Boiss plant extract and the sol–gel technique. The peaks corresponding to (111), (200), (220), (311) and (222) diffraction planes (JCPDS Card No.73-

Fig. 5 Rate constant calculated for dye degradation reaction following a pseudo-first order

Fig. 7 XRD patterns of synthesized NiO-NPs in air at different temperatures

1523) [57] indicated the formation of NiO-NPs with cubic crystal structures of fcc [58]. The pure crystalline structures of NiO-NPs can be confirmed since there were no clear impurity peaks that could be detected throughout XRD charts [59]. The crystallite size was designed in agreement with the following Debye–Scherrer formula, Eq. (9) [50, 60, 61].

$$D = \frac{k\lambda}{\beta \cos \theta} \tag{9}$$

where D is the particle size (nm), $k = 0.94$ would be a crystallized form factor, λ is the wavelength (0.154 nm), β represents the highest width at half maximum of the peak (rad), and θ is the diffraction angle (°).

The crystallite sizes measured to be about 18–43 nm could be caused by the existence of various phytochemicals in the salvia macrosiphon Boiss plant extract, which functions as a capping agent. The sizes of nanoparticles at the temperature of 300, 400, 500 and 600 °C were observed to be about 18, 27, 39 and 43 nm, respectively. Therefore, the appearance of nanometal oxides was in good agreements with the size of particles obtained from FESEM image (30.7 nm) [62]. By enhancing the calcination temperature, an increase in the peak intensity was observed, along with a decrease in the peak width and also an increase in the size of nanoparticles, which is indicative of the crystallinity of synthesized nanoparticles [63]. The sizes of nanoparticles were estimated and are exhibited in Table 1.
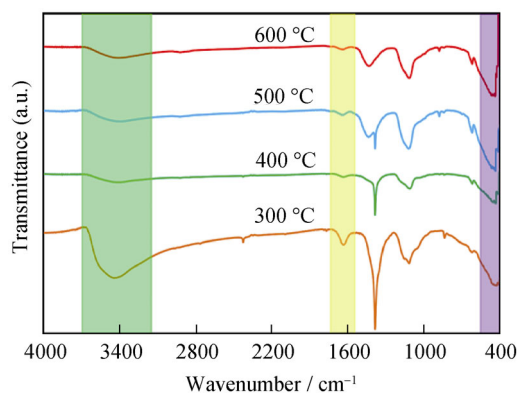
Fig. 8 FTIR spectra of synthesized NiO-NPs in air at different temperatures

### 3.6 FTIR analysis of NiO-NPs

Figure 8 exhibits the results of FTIR analysis to establish the functional groups of NiO-NPs synthesized by the usage of salvia plant extract throughout the region of 400–4000 cm^{-1}. The main bands were observed to exist at 3483, 2017, 1651, 1398, 1130 and 420 cm^{-1}. The vibrations at 3483 and 1651 cm^{-1} seemed to be associated with the ν (O–H) mode of (H-bonded) water molecules and δ (OH), respectively. Normally, the remaining water and hydroxyl groups were apparent within the NiO-NPs and consequently, we supposed that the bands at 2017 and 1651 cm^{-1} are associated with CO_2 and C=C stretching vibrations, respectively [64]. The band at 1130 cm^{-1} was allocated to the first overtone that belonged to the major vibration. The existing peak at 1398 cm^{-1} was the representative of N=O stretching frequency induced by a trace amount of nitrate. The absorption band in the range of 420–500 cm^{-1} could be related to the Ni–O stretching vibration bands in NiO-NPs [65, 66].

3.7 UV–Vis results

Figure 9a illustrates UV–Vis spectra and gap band of NiO-NPs. The as-prepared nanoparticles were described through the usage of UV–Vis spectrum at calcination temperatures of 300, 400, 500 and 600 °C throughout the range of 200–800 nm. The spectrums revealed the existence of absorption peaks at 298, 302, 310 and 315 nm, which could

Table 1 Comparison of particles size of as-synthesized NiO-NPs

Temperature/ °C	2θ/(°)	Full width at half maximum (FWHM)/rad	Particle size/nm	Identification
300	42.84	0.472	18	fcc(NiO)
400	42.84	0.314	27	fcc(NiO)
500	42.88	0.216	39	fcc(NiO)
600	42.84	0.196	43	fcc(NiO)
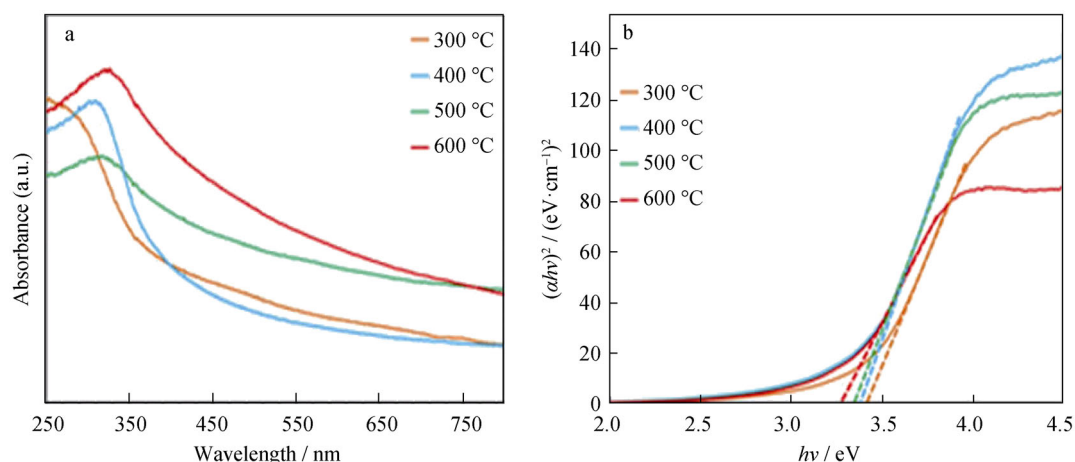
Fig. 9 UV–Vis absorption spectra of **a** NiO-NPs and **b** band gap of prepared NiO-NPs

be attributed to the essential band-gap attraction of NiO-NPs caused by the electron transitions of VB to CB [O (2p) and thus to Ni (3d)] [67]. In other words, the absorption bands in these areas are the outcomes of ligand to metal charge transfer (LMCT) transition (direct transition). The energy band gap of different sintering temperatures in regard to the NiO-NPs can be calculated through the utilization of Tauc equation, Eq. (10).

$$(\alpha h v)^n = A(h v - E_g) \tag{10}$$

where E_g is the gap band energy, $h v$ (eV) is the photon energy, α is the absorption coefficient, A represents a constant and $n = 2$ in direct transition, whereas $n = 1/2$ in indirect transition. By applying Eq. (10) and considering $n = 2$, since NiO is known to be a straight band-gap semiconductor, the energy band gap of the prepared NiO-NPs was calculated and is demonstrated in Table 2. The energy band values were observed to be close to the previously reported values [68]. Based on the Tauc equation, Fig. 9b explains the diagram of $(\alpha h v)^n$ in terms of $h v$; the values of E_g were determined by extrapolating the linear regions of these plots. Furthermore, particles were observed to become smaller as E_g increased, which could be caused by the chemical weaknesses that result in the creation of a new energy level [66, 69].

3.8 FESEM/EDX study

Figure 10 displays FESEM and EDX analysis of NiO-NPs synthesized via the utilization of salvia plant extract at 400 °C. It can be clearly perceived that the NiO-NPs were uniformly distributed while being homogenous and spherical as well [70]. The purity of NiO-NPs was confirmed by the means of EDX, which is capable of accurately measuring Ni and O along with displaying the Ni and O peaks without any impurities [71]. To be stated differently, the phenomenon of nanoparticles aggregation is an important and fundamental subject when its association with many applications of nanoparticles is considered; therefore, it can be observed that the NiO-NPs produced by the usage of salvia were obviously separated with a homogenous morphology. This fact indicated the assistant suggestion for the production of NiO that can be taken into consideration along with XRD and FTIR studies [72].

3.9 VSM analysis of NiO-NPs

Figure 11 illustrates the magnetic structures of NiO-NPs produced by the application of salvia plant extracts and measured through the means of VSM in regard to the calcination sample at 400 °C. The magnetization performance of NiO-NPs was studied by utilizing the foreign magnetic field, which exists from − 1 T to + 1 T, at room temperature. By observing the curve in Fig. 11, it can be stated that there were no any signs of widespread that could be measured in a remanent curve, meaning that this particular curve did not cut the M and H lines at any point. Therefore, it can be presumed that the remanent (M_r) and coercivity (H_c) of both samples were zero, and thus, it can be categorized as superparamagnetic (week ferromagnetic) [73, 74]. In accordance with Fig. 11, there was clearly no hysteresis in the M–H curve and this phenomenon, which is

Table 2 UV–Vis spectra of NiO-NPs at different temperatures

Temperature/ °C	Wavelength/nm	Absorbance	Energy gap/eV
300	298	1.1	3.9
400	302	1.2	3.3
500	310	1.1	3.0
600	315	1.0	2.9
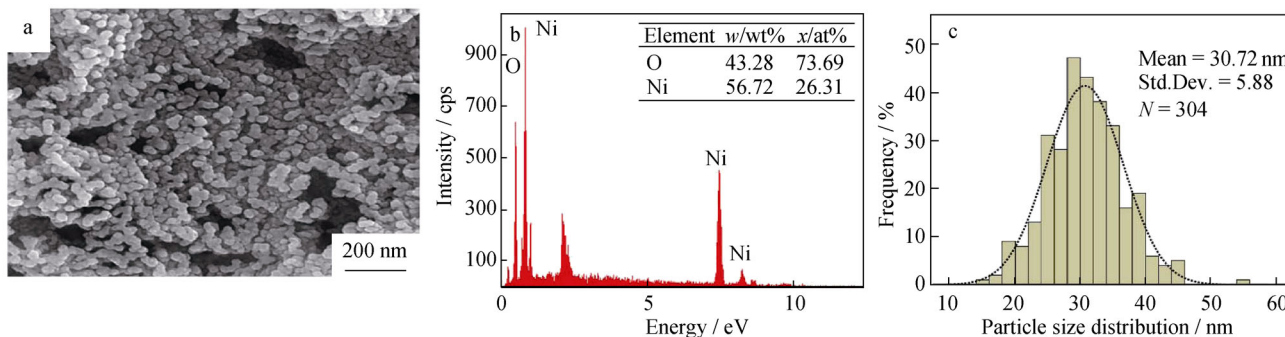
Fig. 10 a FESEM image, **b** EDX analysis and **c** particle size analysis (PSA) of prepared NiO-NPs at 400 °C (Std. Dev. being Standard deviation)
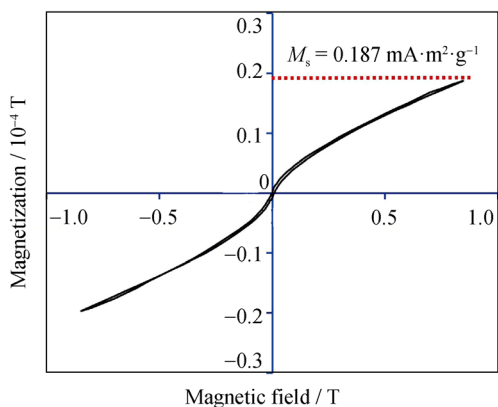
Fig. 11 VSM measurement of prepared NiO-NPs at 400 °C
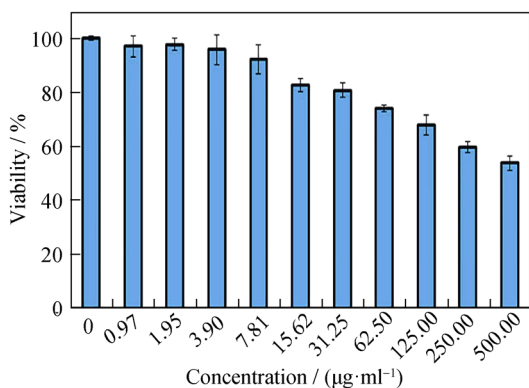
Fig. 12 Cell viability of Neuro2A cells measured by MTT assay

assigned to the single-spatialization of magnetic particles, is probably the reason behind the minor size of nanoparticles [75, 76].

3.10 Evaluation of cytotoxicity studies using NiO-NPs

The cytotoxicity discoveries of NiO-NPs are explained in Fig. 12. We have estimated the cytotoxic influence of produced nanoparticles on the Neuro2A cells lines. The diluted ranges of synthesized NiO extract, which was appended to each plate, were 500.00, 250.00, 125.00, 62.50, 31.20, 15.60, 7.80, 3.90, 1.90 and 0.97 $\mu g \cdot ml^{-1}$. The investigation samples were utilized by a specified amount of cells, while the cytotoxicity for each concentration was evaluated through the application of MTT assay [77]. The absorption of the solution gained by mixing the mentioned crystals with DMSO was determined to be at 545 nm by the employment of a spectrophotometer. In total, the cell viability seemed to decrease as the concentration of nanoparticles increased, while the reduction was observed to be dose dependent [57]. However, the 3-(4,5-dimethylthiazol-2-yl)-2,5-diphenyltetrazolium bromide (MTT) assay in regard to Neuro2A cells viability was detected to be 53% and upon the application of 500.00 $\mu g \cdot ml^{-1}$ of NiO-NPs that was produced by salvia plant extract, the mentioned percentage faced an increase toward the maximum of 92% at the concentration of 7.80 $\mu g \cdot ml^{-1}$. Although the impact mechanism of particular factors on cytotoxicity effects has not been clearly understood, there are some reports suggesting that the released metal ions [78] of nanometal oxides show that the major cytotoxicity publication of Ni^{2+} will be more significant in nano-sized NiO and thus will face a greater decrease in its cytotoxicity than the micron-sized particles [79]. In addition, the greater cytotoxicity of NiO-NPs, in comparison with the Neuro2A cell lines, might be also related to their decreased particle size. Therefore, the NiO-NPs were synthesized by the usage of salvia plant extract as their fuel apparently possessed high cytotoxicity activities, while the results from Fig. 12 proved that as the concentration of NiO-NPs increased, a reduction will occur in absorption and cell viability as well. The decrease in particle size, particular surface region and the freedom of Ni^{2+} caused the maximum cytotoxicity influence throughout the current research. The results in Fig. 12 displayed the significant toxic effects of NiO-NPs on the remains of Neuro2A cells at high concentrations and a negligible effect on the low concentrations of this particular cell line.

4 Conclusion

In this study, NiO-NPs were synthesized through a sol–gel method, which involved the use of salvia macrosiphon Boiss extract as a limiting agent. The nanoparticles were calcinated at different temperatures of 300, 400, 500 and 600 °C. The characterization approaches of FTIR, UV–Vis, XRD, FESEM-EDX, TGA/DTA and VSM were employed to approve the manufacturing, crystallinity and morphology of NiO-NPs. The outcomes of XRD studies indicated that the heightening of calcination temperature can lead to an increase in the size of nanoparticles and consequently, the lowest calcination temperature (400 °C) caused the smallest size (27 nm) and best crystallinity of NiO-NPs. The FTIR results suggested the existence of particular functional groups that might be answerable for the synthesis of NiO-NPs. The appearances of nickel and oxygen elements were established with EDX figure, while FESEM images confirmed that the nanoparticles contained a uniformed distribution and spherical shape. In accordance with the photocatalyst test, NiO-NPs exhibited the best functionality in the role of a photocatalyst throughout the degeneration of MB under UV-A (11 W) light radiation. Cytotoxicity studies were performed on Neuro2A cell lines by the MTT procedure, and the obtained results proposed that the percentage of cell viability was successfully reduced. Therefore, NiO-NPs can be recommended as a photocatalyst for eliminating pollutants, as well as an excellent case for cancer treatment.

References

[1] Peck MA, Langell MA. Comparison of nanoscaled and bulk NiO structural and environmental characteristics by XRD, XAFS, and XPS. Chem Mater. 2012;24(23):4483.

[2] Farhadi S, Roostaei-Zaniyani Z. Simple and low-temperature synthesis of NiO nanoparticles through solid-state thermal decomposition of the hexa(ammine)Ni(II) nitrate, $[Ni(NH_3)_6](NO_3)_2$, complex. Polyhedron. 2011;30(7):1244.

[3] Hosny NM. Synthesis, characterization and optical band gap of NiO nanoparticles derived from anthranilic acid precursors via a thermal decomposition route. Polyhedron. 2011;30(3):470.

[4] Deraz N, Selim M, Ramadan M. Processing and properties of nanocrystalline Ni and NiO catalysts. Mater Chem Phys. 2009;113(1):269.

[5] Maia AOG, Meneses CT, Menezes AS, Flores WH, Melo DMA, Sasaki JM. Synthesis and X-ray structural characterization of NiO nanoparticles obtained through gelatin. J Non-Cryst Solids. 2006;352(32–35):3729.

[6] Pugazhendhi A, Prabhu R, Muruganantham K, Shanmuganathan R, Natarajan S. Anticancer, antimicrobial and photocatalytic activities of green synthesized magnesium oxide nanoparticles (MgONPs) using the aqueous extract of Sargassum wightii. J Photochem Photobiol B. 2019;190:86.

[7] Whitesides GM. Nanoscience, nanotechnology, and chemistry. Small. 2005;1(2):172.

[8] Yuko I, Naoto W, Junichiro Y, Saori Y, Yoshihide K, Eriko K, Hiroyuki T. Magnetic properties of NiO nanoparticles. Physica B. 2003;329:862.

[9] Pankhurst QA, Connolly J, Jones S, Dobson J. Applications of magnetic nanoparticles in biomedicine. J Phys D Appl Phys. 2003;36(13):R167.

[10] Amani-Beni Z, Nezamzadeh-Ejhieh A. NiO nanoparticles modified carbon paste electrode as a novel sulfasalazine sensor. Anal Chim Acta. 2018;1031:47.

[11] Hwang SC, Yoo SJ, Shin J, Cho YH, Jang JH, Cho E, Sung YE, Nam SW, Lim TH, Lee SC, Kim SK. Supported core@shell electrocatalysts for fuel cells: a close encounter with reality. Sci Rep. 2013;3:1309.

[12] Cheng J, Liping D, Zhang B, Ping S, Guangyao M. Properties and microstructure of NiO/SDC materials for SOFC anode applications. Rare Met. 2007;26(2):110.

[13] Adekunle AS, Oyekunle JAO, Oluwafemi OS, Joshua AO, Makinde WO, Ogunfowokan AO, Eleruja MA, Ebenso Eno E. Comparative catalytic properties of $Ni(OH)_2$ and NiO nanoparticles towards the degradation of nitrite (NO_2-) and nitric oxide (NO). Int J Electrochem Sci. 2014;9(6):3008.

[14] Darroudi M, Ahmad MB, Zak AK, Zamiri R, Hakimi M. Fabrication and characterization of gelatin stabilized silver nanoparticles under UV-light. Int J Mol Sci. 2011;12(9):6346.

[15] Amity Institute of Biotechnology AUUPLC, Gomti Nagar Extension, Lucknow UP, INDIA. A review on nanoparticles: their synthesis and types. Res J Recent Sci. 2015;4:9.

[16] Xiang L, Deng XY, Jin Y. Experimental study on the synthesis of NiO nanoparticles. Scr Mater. 2002;47(4):219.

[17] Pradeep T. Noble metal nanoparticles for water purification: a critical review. Thin Solid Films. 2009;517(24):6441.

[18] Bahadur J, Sen D, Mazumder S, Ramanathan S. Effect of heat treatment on pore structure in nano-crystalline NiO: a small angle neutron scattering study. J Solid State Chem. 2008;181(5):1227.

[19] Li W, Haldar P. Highly active carbon supported core-shell PtNi@Pt nanoparticles for oxygen reduction reaction. Electrochem Solid State Lett. 2010;13(5):B47.

[20] Wu Y, He Y, Wu T, Weng W, Wan H. Effect of synthesis method on the physical and catalytic property of nanosized NiO. Mater Lett. 2007;61(13):2679.

[21] Bouremana A, Guittoum A, Hemmes M, Martínez-Blanco D, Gorria P, Blanco J, Benrekaa N. Microstructure, morphology and magnetic properties of Ni nanoparticles synthesized by hydrothermal method. Mater Chem Phys. 2015;160:435.

[22] Wang SF, Shi LY, Feng X, Ma SR. Eutectic assisted synthesis of nanocrystalline NiO through chemical precipitation. Mater Lett. 2007;61(7):1549.

[23] Parsaee Z. Synthesis of novel amperometric urea-sensor using hybrid synthesized NiO-NPs/GO modified GCE in an aqueous solution of cetrimonium bromide. Ultrason Sonochem. 2018;44:120.

[24] Lai TL, Shu YY, Huang GL, Lee CC, Wang CB. Microwave-assisted and liquid oxidation combination techniques for the preparation of nickel oxide nanoparticles. J Alloys Compd. 2008;450(1–2):318.

[25] Qamara M, Gondal MA, Yamania ZH. Synthesis of nanostructured NiO and its application in laser-induced photocatalytic reduction of Cr(VI) from the water. J Mol Catal A Chem. 2011;341(1–2):83.

[26] Teoh LG, Li KD. Synthesis and characterization of NiO nanoparticles by sol–gel method. Mater Trans. 2012;53:2135.

[27] Zhang W, Liu HX, Hu C, Zhu XJ, Li YX. Preparation of layered oxide Li $(Co_{1/3}Ni_{1/3}Mn_{1/3})O_2$ via the sol–gel process. Rare Met. 2008;27(2):158.

[28] Della Gaspera E, Bello V, Mattei G, Martucci A. SiO_2 mesoporous thin films containing Ag and NiO nanoparticles synthesized combining sol–gel and impregnation techniques. Mater Chem Phys. 2011;131(1–2):313.

[29] Akbari A, Khammar M, Taherzadeh D, Rajabian A, Zak AK, Darroudi M. Zinc-doped cerium oxide nanoparticles: sol–gel synthesis, characterization, and investigation of their in vitro cytotoxicity effects. J Mol Struct. 2017;1149:771.

[30] Jeevanandam P, Pulimi VRR. Synthesis of nanocrystalline NiO by sol–gel and homogeneous precipitation methods. Indian J Chem. 2012;51A(04):586.

[31] Derikvandi H, Nezamzadeh-Ejhieh A. Increased photocatalytic activity of NiO and ZnO in the photodegradation of a model drug aqueous solution: effect of coupling, supporting, particles size and calcination temperature. J Hazard Mater. 2017;321:629.

[32] Ameta P, Kumar A. A comparative study of photocatalytic activity of some coloured semiconducting oxides. Iran J Chem Chem Eng. 2010;29(2):43.

[33] Huang B, Li N, Lin W, Li H. A highly ordered honeycomb-like nickel(III/II) oxide-enhanced photocatalytic fuel cell for effective degradation of bisphenol A. J Hazard Mater. 2018;360:578.

[34] Fernandes DM, Hechenleitner AAW, Silva MF, Lima MK, Bittencourt PRS, Silva R, Melo MAC, Pineda EAG. Preparation and characterization of NiO, Fe_2O_3, $Ni_{0.04}Zn_{0.96}O$, and $Fe_{0.03}Zn_{0.97}O$ nanoparticles. Mater Chem Phys. 2009;118(2–3):447.

[35] He H, Yang S, Yu K, Ju Y, Sun C, Wang L. Microwave induced catalytic degradation of crystal violet in nano-nickel dioxide suspensions. J Hazard Mater. 2010;173(1):393.

[36] Alnarabiji MS, Yahya N, Hamed Y, Ardakani SEM, Azizi K, Klemeš JJ, Abdullah B, Tasfy SFH, Abd Hamid ShB, Nashed O. Scalable bio-friendly method for production of homogeneous metal oxide nanoparticles using green bovine skin gelatin. J Clean Prod. 2017;162:186.

[37] Lai TL, Liu JY, Yong KF, Shu YY, Wang CB. Microwave-enhanced catalytic degradation of 4-chlorophenol over nickel oxides under low temperature. J Hazard Mater. 2008;157(2):496.

[38] Ejhieh AN, Khorsandi M. Photodecolorization of eriochrome black T using NiS–P zeolite as a heterogeneous catalyst. J Hazard Mater. 2010;176(1–3):629.

[39] Vasantharaj S, Sathiyavimal S, Saravanan M, Senthilkumar P, Gnanasekaran K, Shanmugavel M, Manikandan E, Pugazhendhi A. Synthesis of eco-friendly copper oxide nanoparticles for fabrication over textile fabrics: characterization of antibacterial activity and dye degradation potential. J Photochem Photobiol B. 2019;191:143.

[40] Makarov VV, Love AJ, Sinitsyna OV, Makarova SS, Yaminsky IV, Taliansky ME, Kalinina NO. "Green" nanotechnologies: synthesis of metal nanoparticles using plants. Acta Nat. 2014;6(1):35.

[41] Wu Y, He Y, Wu T, Chen T, Weng W, Wan H. Influence of some parameters on the synthesis of nanosized NiO material by a modified sol–gel method. Mater Lett. 2007;61(14–15):3174.

[42] Singh P, Kim YJ, Zhang D, Yang DC. Biological synthesis of nanoparticles from plants and microorganisms. Trends Biotechnol. 2016;34(7):588.

[43] Jacob JM, Rajan R, Aji M, Kurup GG, Pugazhendhi A. Bio-inspired ZnS quantum dots as efficient photocatalysts for the degradation of methylene blue in the aqueous phase. Ceram Int. 2018;11:182.

[44] Hu H, Wang M, Deng C, Chen J, Wang A, Le H. Satellite-like CdS nanoparticles anchoring onto porous NiO nanoplates for enhanced visible-light photocatalytic properties. Mater Lett. 2018;224:75.

[45] Ramesh M, Rao MPC, Anandan S, Nagaraja H. Adsorption and photocatalytic properties of NiO nanoparticles synthesized via a thermal decomposition process. J Mater Res. 2018;33(5):601.

[46] Domen K, Kudo A, Onishi T. Mechanism of photocatalytic decomposition of water into H_2 and O_2 over NiO $SrTiO_3$. J Catal. 1986;102(1):92.

[47] Li Y, Niu J, Yin L, Wang W, Bao Y, Chen J, Duan Y. Photocatalytic degradation kinetics and mechanism of pentachlorophenol based on superoxide radicals. J Environ Sci. 2011;23(11):1911 (**China**).

[48] Dong C, Xiao X, Chen G, Guan H, Wang Y. Synthesis and photocatalytic degradation of methylene blue over PN junction Co_3O_4/ZnO core/shell nanorods. Mater Chem Phys. 2015;155:1.

[49] Abdul Rahman I, Ayob M, Radiman S. Enhanced photocatalytic performance of NiO-decorated ZnO nanowhiskers for methylene blue degradation. J Nanotechnol. 2014. https://doi.org/10.1155/2014/212694.

[50] Fathima JB, Pugazhendhi A, Oves M, Venis R. Synthesis of eco-friendly copper nanoparticles for augmentation of catalytic degradation of organic dyes. J Mol Liq. 2018;260:1.

[51] Wang X, Mao H, Shan Y. Enhanced photocatalytic behavior and excellent electrochemical performance of hierarchically structured NiO microspheres. RSC Adv. 2014;4(67):35614.

[52] Carreon ML, Carreon HG, Espino-Valencia J, Carreon MA. Photocatalytic degradation of organic dyes by mesoporous nanocrystalline anatase. Mater Chem Phys. 2011;125(3):474.

[53] Saratale RG, Ghodake GS, Shinde SK, Cho SK, Saratale GD, Pugazhendhi A, Bharagava RN. Photocatalytic activity of CuO/$Cu(OH)_2$ nanostructures in the degradation of reactive green 19A and textile effluent, phytotoxicity studies and their biogenic properties (antibacterial and anticancer). J Environ Manage. 2018;223:1086.

[54] Nezamzadeh-Ejhieh A, Ghanbari-Mobarakeh Z. Heterogeneous photodegradation of 2, 4-dichlorophenol using FeO doped onto nano-particles of zeolite P. J Ind Eng Chem. 2015;21:668 (**Washington, DC**).

[55] Hassanpour M, Safardoust-Hojaghan H, Salavati-Niasari M. Rapid and eco-friendly synthesis of NiO/ZnO nanocomposite and its application in decolorization of dye. J Mater Sci Mater Electron. 2017;28(15):10830.

[56] Rakshit S, Ghosh S, Chall S, Mati SS, Moulik S, Bhattacharya SC. Controlled synthesis of spin glass nickel oxide nanoparticles and evaluation of their potential antimicrobial activity: a cost-effective and eco-friendly approach. RSC Adv. 2013;3(42):19348.

[57] Ahamed M, Ali D, Alhadlaq HA, Akhtar MJ. Nickel oxide nanoparticles exert cytotoxicity via oxidative stress and induce an apoptotic response in human liver cells (HepG2). Chemosphere. 2013;93(10):2514.

[58] Karthik K, Dhanuskodi S, editors. Structural and optical properties of microwave assisted CdO-NiO nanocomposite. In: AIP Conference Proceedings 2016. 2016;1731(1):050021.

[59] Wang X, Pu H, Hu D, Zang Y, Hu J, Yang Y. Chen ChPreparation of p-NiO/n-SiC heterojunction on the 4H-SiC substrate. Mater Lett. 2018;227:315.

[60] Shabani-Nooshabadi M, Tahernejad-Javazmi F. Rapid and fast strategy for the determination of glutathione in the presence of vitamin B 6 in biological and pharmaceutical samples using a nanostructure-based electrochemical sensor. RSC Adv. 2015;5(69):56255.

[61] Saleem S, Ahmed B, Khan MS, Al-Shaeri M, Musarrat J. Inhibition of growth and biofilm formation of clinical bacterial isolates by NiO nanoparticles synthesized from *Eucalyptus globulus* plants. Microb Pathog. 2017;111:375.

[62] Rahman MA, Radhakrishnan R, Gopalakrishnan R. Structural, optical, magnetic and antibacterial properties of Nd doped NiO nanoparticles prepared by co-precipitation method. J Alloys Compd. 2018. https://doi.org/10.1016/j.jallcom.2018.01.298.

[63] Senobari S, Nezamzadeh-Ejhieh A. A pn junction NiO-CdS nanoparticles with enhanced photocatalytic activity: a response surface methodology study. J Mol Liq. 2018;257:173.

[64] Patel KN, Deshpande M, Chauhan K, Rajput P, Gujarati VP, Pandya S, Sathe V, Chaki SH. Effect of Mn doping concentration on structural, vibrational and magnetic properties of NiO nanoparticles. Adv Powder Technol. 2018;29(10):2394.

[65] Vishnukumar P, Saravanakumar B, Ravi G, Ganesh V, Guduru RK, Yuvakkumar R. Synthesis and characterization of NiO/Ni$_3$V$_2$O$_8$ nanocomposite for supercapacitor applications. Mater Lett. 2018;219:114.

[66] Gondal M, Saleh TA, Drmosh Q. Synthesis of nickel oxide nanoparticles using pulsed laser ablation in liquids and their optical characterization. Appl Surf Sci. 2012;258(18):6982.

[67] Klochko N, Klepikova K, Zhadan D, Petrushenko S, Kopach V, Khrypunov G, Lyubov V, Dukarov S, Nikitin V, Maslak M, Zakovorotniy A, Khrypunova A. Structure, optical, electrical and thermoelectric properties of solution-processed Li-doped NiO films grown by SILAR. Mater Sci Semicond Process. 2018;83:42.

[68] Jahromi SP, Huang N, Muhamad M, Lim H. Green gelatine-assisted sol–gel synthesis of ultrasmall nickel oxide nanoparticles. Ceram Int. 2013;39(4):3909.

[69] Roy HS. Polymer composites based on functionalized metal analogs incorporated with ionic liquids for electrochemical applications. Dhaka: University of Dhaka; 2018.

[70] Oves M, Aslam M, Rauf MA, Qayyum S, Qari HA, Khan MS, Alam MZ, Tabrez S, Pugazhendhi A, Ismail IMI. Antimicrobial and anticancer activities of silver nanoparticles synthesized from the root hair extract of Phoenix dactylifera. Mater Sci Eng C. 2018;89:429.

[71] Sadeghi M, Ghaedi H, Yekta S, Babanezhad E. Decontamination of toxic chemical warfare sulfur mustard and nerve agent simulants by NiO NPs/Ag-clinoptilolite zeolite composite adsorbent. J Environ Chem Eng. 2016;4(3):2990.

[72] Barakat NA, Abdelkareem MA, El-Newehy M, Kim HY. Influence of the nanofibrous morphology on the catalytic activity of NiO nanostructures: an effective impact toward methanol electrooxidation. Nanoscale Res Lett. 2013;8(1):402.

[73] Das RK, Golder AK. Use of plant-based analytes for the synthesis of NiO nanoparticles in catalyzing electrochemical H$_2$O$_2$ production. J Electron Chem. 2018;823:9.

[74] Soleimani E, Mohammadi M. Synthesis, characterization and properties of polystyrene/NiO nanocomposites. J Mater Sci Mater Electron. 2018;29(11):9494.

[75] Seto T, Akinaga H, Takano F, Koga K, Orii T, Hirasawa M. Magnetic properties of monodispersed Ni/NiO core-shell nanoparticles. J Phys Chem B. 2005;109(28):13403.

[76] Ibrahim E, Abdel-Rahman LH, Abu-Dief AM, Elshafaie A, Hamdan SK, Ahmed A. The synthesis of CuO and NiO nanoparticles by facile thermal decomposition of metal-Schiff base complexes and an examination of their electric, thermoelectric and magnetic properties. Mater Res Bull. 2018;107:492.

[77] Siddiqui MA, Ahamed M, Ahmad J, Khan MM, Musarrat J, Al-Khedhairy AA, Alrokayan SA. Nickel oxide nanoparticles induce cytotoxicity, oxidative stress, and apoptosis in cultured human cells that is abrogated by the dietary antioxidant curcumin. Food Chem Toxicol. 2012;50(3–4):641.

[78] Karthik K, Dhanuskodi S, Gobinath C, Prabukumar S, Sivaramakrishnan S. Nanostructured CdO–NiO composite for multifunctional applications. Food Chem Toxicol. 2018;112:106.

[79] Mariam AA, Kashif M, Arokiyaraj S, Bououdina M, Sankaracharyulu M, Jayachandran-M M, Hashim U. Bio-synthesis of NiO and Ni nanoparticles and their characterization. J Nanomater Biostruct. 2014;9(3):1007.